

$\text{Cu}_2(1,4\text{-diazacycloheptane})_2\text{Cl}_4$ is not a Spin Ladder

M. B. Stone¹, J. Rittner¹, Y. Chen¹, H. Yardimci¹, D. H. Reich¹, C. Broholm^{1,2}, D. V. Ferraris³, and T. Lectka³

¹Department of Physics and Astronomy, The Johns Hopkins University, Baltimore, MD 21218

²National Institute of Standards and Technology, Gaithersburg, MD 20899

³Department of Chemistry, The Johns Hopkins University, Baltimore, MD 21218

(May 20, 2019)

Inelastic neutron scattering measurements are reported for the strongly dimerized quantum antiferromagnetic material $\text{Cu}_2(1,4\text{-diazacycloheptane})_2\text{Cl}_4$ (CuHPCl). Experiments were carried out on both a deuterated powder and hydrogenated single crystals. The results confirm the existence of a band of magnetic excitations in this system in the energy range $0.8 \text{ h}\bar{1} \text{ } 1.4 \text{ m eV}$ previously observed for hydrogenated powder samples. The wavevector dependence of the scattering intensity is inconsistent with the currently accepted spin-ladder model of the antiferromagnetic interactions in this system. At $T = 1.6 \text{ K}$, the excitation spectrum contains two modes. These modes show dispersion both parallel and perpendicular to the putative ladder direction in the crystalline ac -plane. A analysis based on the first moment sum rule indicates that the dimer bond is different than previously supposed, and that geometrical frustration is important in this system.

I. INTRODUCTION

Low-dimensional antiferromagnets are excellent systems for probing many-body physics in regimes where quantum fluctuations play a significant role. An important class of such systems are the $S=1/2$ spin-gap systems. These have no static magnetic order in the absence of a magnetic field, but have a cooperative singlet ground state and coherent triplet spin excitations. Among the simplest of these systems are those that behave as collections of strongly coupled pairs of spins (dimers), with weaker inter-dimer couplings. Depending on the nature of the inter-dimer interactions, a number of interesting interacting dimer networks are possible. These include alternating bond spin chains as found in $\text{Cu}(\text{NO}_3)_2 \cdot 2.5\text{D}_2\text{O}$ ¹ and $(\text{VO})_2\text{P}_2\text{O}_7$,^{2,5} two-leg spin-ladders as in $(\text{La;Sr;Ca})_{14}\text{Cu}_{24}\text{O}_{41}$,^{6,8} (which also has dimerized chains) as well as a variety of two-dimensional or three-dimensional networks such as $\text{Cs}_3\text{C}_2\text{B}_2\text{R}_9$,⁹ $\text{BaCuSi}_2\text{O}_6$,¹⁰ KCuCl_3 ,¹¹ $(\text{C}_4\text{H}_{12}\text{N}_2)\text{Cu}_2\text{Cl}_6$,¹² and $\text{SrCu}_2(\text{BO}_3)_2$.¹³

Another material that has received considerable attention is $\text{Cu}_2(1,4\text{-diazacycloheptane})_2\text{Cl}_4$ (CuHPCl).^{14,27} Measurements of the magnetization, magnetic susceptibility, and specific heat show that this system has a spin gap 0.9 m eV , a magnetic bandwidth of approximately 0.5 m eV , and a saturation field $H_{\text{C}2} = 13.2 \text{ T}$. Based on these measurements and the nature of the crystal structure, it was proposed that CuHPCl is a two-leg spin ladder composed of coupled dimers, with the intradimer bonds of strength $J_1 = 1.14 \text{ m eV}$ forming the rungs, and interdimer bonds of strength $J_2 = 0.2J_1$ forming the legs of the ladders.¹⁶ Subsequent experimental results have generally been interpreted in terms of this model, and this system has been the inspiration for a number of theoretical studies.^{28,36}

Despite this extensive body of work, the true nature of the inter-dimer spin interactions in CuHPCl has never been conclusively demonstrated. In strongly dimerized

antiferromagnetic spin systems, identification of the microscopic spin Hamiltonian is difficult without measurements that probe spatial correlations directly.⁵ In CuHPCl, for example, the susceptibility and specific heat data are equally well described by spin-ladder, alternating chain, and coupled-bilayer models.²⁸ Some evidence that the two-leg ladder model might in fact not be appropriate for CuHPCl came from a previous inelastic neutron scattering experiment¹⁹ on a powder sample, where we found that the wavevector-integrated magnetic scattering intensity did not show the characteristic van Hove singularities expected for the magnetic density of states of a one-dimensional spin system. In this measurement, the wavevector dependence of the energy-integrated magnetic scattering was also inconsistent with the predictions of the ladder model. However, interpretation of this result was complicated by the coarse wavevector resolution of the instrument employed, and the presence of hydrogen in the sample, which resulted in a large, non-magnetic background signal. In this paper, we report inelastic neutron scattering measurements performed both on a deuterated powder with improved wavevector resolution and on hydrogenated single crystals. The powder and single-crystal measurements are each independently inconsistent with the spin-ladder model. The powder data indicate that the strongest dimer bond is different from that of the ladder model. The single-crystal measurements show the presence of two modes within the 0.5 m eV bandwidth, a feature not predicted by the spin-ladder model. Most importantly, these modes exhibit dispersion in all directions in the $(h0l)$ reciprocal lattice plane, which shows that the magnetic coupling in CuHPCl is at least two-dimensional in nature. Both sets of measurements indicate that geometrical frustration may play an important role in this material.

II. EXPERIMENTAL TECHNIQUES

CuHfCl is monoclinic with space group $P2_1/c$ and room temperature lattice constants $a = 13.406(3)$, $b = 11.454(2)$, $c = 12.605(3)$, and $\beta = 115.01(2)^\circ$.¹⁴ The powder sample studied consisted of 5.87 grams of deuterated CuHfCl. To produce this sample, perdeuterated 1,4-diazacycloheptane was first prepared following a previously published method.³⁷ The d_6 -dibromopropane and $N;N^0$ -dibenzylethylene- d_4 -diamine precursors required for this synthesis were prepared from commercially available 1,3- d_6 -propanediol and ethylene- d_4 -diamine, respectively. The CuHfCl powder was obtained by rapid cooling from 40 C to 0 C of 1:1 molar solutions of anhydrous $CuCl_2$ and the deuterated 1,4-diazacycloheptane dissolved in the minimum amount of deuterated methanol. Prompt gamma neutron activation analysis performed on a portion of the sample confirmed 95.0(1)% deuteration.

The single crystal measurements were performed on a composite sample with a total mass of 110 mg. The sample consisted of four hydrogenated single crystals mutually aligned to within 4.5 degrees. These crystals were obtained by diffusive growth from $CuCl_2$ and 1,4-diazacycloheptane in methanol.²⁵ We have produced crystals as large as 33 mg using this method.

Inelastic neutron scattering measurements on both the powder and single-crystal samples were performed using the SPINS cold neutron triple axis spectrometer at the National Institute of Standards and Technology in Gaithersburg, Maryland. For the powder experiment, the horizontal beam collimation before the sample was $50^\circ=k_i(A^{-1}) - 80^\circ$. Scattered neutrons in the energy range $2.6 \text{ meV} < E_f < 3.7 \text{ meV}$ were measured with a 23 cm wide by 15 cm high pyrolytic graphite analyzer (PG (002)) at a distance of 91 cm from the sample position. The analyzer was followed by an 80° radial collimator and a position-sensitive detector. Cooled Be and BeO filters were employed before and after the sample, respectively. Data were collected by scanning the scattering angle 2θ in the range 7° to 114° at fixed incident energy E_i . Scans at $E_i = 4.0, 4.34, \text{ and } 4.84 \text{ meV}$ probed inelastic scattering for energy transfer $0.4 \text{ meV} < \hbar\omega < 2.09 \text{ meV}$ and momentum transfer $0.2 A^{-1} < Q < 2.35 A^{-1}$, with average full width at half maximum (FWHM) resolutions $\hbar\omega = 0.21 \text{ meV}$ and $Q = 0.028 A^{-1}$. The corresponding FWHM resolution ellipse³⁸ is shown in Fig. 1(a). Backgrounds due to incoherent scattering at the analyzer and low-angle air scattering of the incident neutron beam were measured separately. After subtracting these backgrounds, the data were converted to the normalized scattering intensity $I(Q; \hbar\omega)$ using the measured incoherent elastic scattering from the sample following the procedure detailed in Ref.¹⁹.

For the single-crystal measurements, the horizontal beam collimation before the sample was $50^\circ=k_i(A^{-1}) - 78^\circ$. A liquid nitrogen cooled BeO filter was placed after the sample and data were collected at fixed energy

$E_f = 3.7 \text{ meV}$ while scanning the incident energy in the range $3.95 \text{ meV} < E_i < 5.45 \text{ meV}$. A horizontally-focusing pyrolytic graphite analyzer was used in conjunction with a single detector. In this configuration, after accounting for the mosaic of the sample, the average instrumental energy resolution for the energy transfer range of 0.75 to 1.25 meV was $\hbar\omega = 0.17(1) \text{ meV}$. Representative values of the projected FWHM wavevector resolution for the constant Q scans performed throughout the measurement are $Q_x = 0.081 A^{-1}$ and $Q_y = 0.065 A^{-1}$ for the components of the wavevector transfer along the principal directions of the resolution ellipse at $Q = (100)$ and $\hbar\omega = 1 \text{ meV}$. Scans at constant wavevector transfer were performed in both the $(h0l)$ and $(hk0)$ reciprocal lattice planes.

III. RESULTS

A. Powder Sample Measurements

Figure 1(a) shows the normalized scattering intensity $I(Q; \hbar\omega)$ for CuHfCl at $T = 0.3 \text{ K}$, obtained by combining measurements at $E_i = 4.84, 4.3, \text{ and } 4.0 \text{ meV}$. This figure was produced by binning the data in bins of size $0.2 \hbar\omega \times 0.2 Q$ and then coarse-grain averaging over the average projected FWHM resolution in energy and wavevector transfer. We observe a pronounced band of scattering intensity in the range of energy transfer $0.8 \text{ meV} < \hbar\omega < 1.4 \text{ meV}$, consistent with our previous measurements on hydrogenated samples.¹⁹ The wavevector averaged scattering intensity

$$I(\hbar\omega) = \frac{\int_{\text{BR}} Q^2 dQ I(Q; \hbar\omega)}{Q^2 dQ} \quad (1)$$

is shown in Fig. 2. Although barely resolved, the data show indications of two distinct maxima. The single-crystal data to be discussed later confirm the presence of two separate modes of magnetic excitations. Within the bandwidth of this local fluctuation spectrum, Fig. 1(a) shows a strong peak near $Q = 0.6 A^{-1}$, and a secondary peak near $Q = 1.3 A^{-1}$. At $T = 30 \text{ K}$, the scattering intensity is diminished throughout the band, as shown in Fig. 1(b). This confirms that the observed scattering intensity is magnetic in origin.

The fact that the magnetic bandwidth in CuHfCl is small compared to the average energy of the magnetic excitations is consistent with the existence of strong dimerization in this material. We now discuss how the wavevector-dependence of the data in Fig. 1(a) can be combined with sum rules to extract information about the relative strengths and geometry of the magnetic couplings in a model-independent manner.

For a powder sample, the magnetic component of $I(Q; \hbar\omega)$ is related to the spherically averaged dynamic spin correlation function $S(Q; \hbar\omega)$ by¹⁹

$$I_m(Q; h!) = 2 \int_{-Z}^Z dQ^0 \text{hd}!^0 R_{Q!}(Q - Q^0; !^0) \int_{-Z}^Z f(Q^0) f(S(Q^0; !^0)); \quad (2)$$

where $R_{Q!}(Q; !)$ is the instrumental resolution function,³⁸ $f(Q)$ is the magnetic form factor for Cu^{2+} , and g is the average g -factor, which is $g = 2.083$ for CuHPCl .¹⁶ The dynamic spin correlation function $S(Q; !)$ is constrained by the total momentum sum rule,

$$\int_{-Z}^Z d^3Q \text{hd}! S(Q; !) = \int_{-Z}^Z d^3Q = S(S+1); \quad (3)$$

Carrying out this integration for the magnetic band of scattering in Fig. 1(a) yields the value 0.7(1), indicating that the observed spectrum contains essentially all of the magnetic spectral weight in this system. Thus in measuring quantities that require knowledge of the full spectrum, it suffices to integrate over the observed magnetic band.

Direct insight into the geometric structure of the spin couplings may be obtained from the first-moment sum rule³⁹

$$\text{hd}! \int_{-Z}^Z d^3Q \text{hd}! S(Q; !) = \int_{-Z}^Z d^3Q \text{hd}! S(Q; !) = \int_{-Z}^Z d^3Q \text{hd}! S(Q; !); \quad (4)$$

Here $\text{hd}!$ is the set of all bond vectors connecting a spin to its neighbors. The Hamiltonian is assumed to take the form

$$H = \sum_{r;d} J_d S_r \cdot S_{r+d} \quad (5)$$

where the set $\text{hd}!$ is chosen so that each unique spin pair enters the summation once. The first moment $\text{hd}! \int_{-Z}^Z d^3Q \text{hd}! S(Q; !)$ of the measured quantity $I_m(Q; h!)$ is related to the spherical average of Eq. 4, and is given by

$$\text{hd}! \int_{-Z}^Z d^3Q \text{hd}! S(Q; !) = \int_{-Z}^Z d^3Q \text{hd}! S(Q; !) = \int_{-Z}^Z d^3Q \text{hd}! S(Q; !); \quad (6)$$

where $d = |d|$.

The first moment $\text{hd}! \int_{-Z}^Z d^3Q \text{hd}! S(Q; !)$ computed from the data in Fig. 1(a) is shown in Fig. 3. In strongly dimerized systems, the term arising from the intradimer bond dominates the first moment.¹ In the two-leg ladder picture of CuHPCl , the intradimer bond is the rung of the ladder, Bond 1 in Table I, with room temperature length $d_1 = 3.422 \text{ \AA}$.¹⁶ As shown by the dashed line in Fig. 3, the Q -dependence arising from inserting d_1 in Eq. 6 is inconsistent with the data. Specifically, the 3.422 \AA bond

yields a maximum at higher Q than is observed in the experiment. Thus, a longer bond (or bonds) must give the dominant contribution to $\text{hd}! \int_{-Z}^Z d^3Q \text{hd}! S(Q; !)$. Fitting the data in Fig. 3 to Eq. 6 with a single, variable bond length d yields $d = 7.5(2) \text{ \AA}$, and the dashed-dotted line shown in Fig. 3. The parameters determined from this fit are given in Table II. As listed in Table I, the CuHPCl crystal structure contains eight distinct Cu-Cu spacings in the range 7 to 7.7 \AA . Thus while this result rules out the rung of the ladder as the strong bond, it does not allow unambiguous identification of the actual dimer.

The fit to the data in Fig. 3 is improved if contributions from two Cu-Cu bonds d and d_1 are included in Eq. 6. This was done with the restriction $d > d_1$, as that is the shortest Cu-Cu spacing in the material. The best combination was found to be $d = 7.5(1) \text{ \AA}$ and $d = d_1$ (see Table II). The resulting fit is shown as a solid line in Fig. 3. We note that in this fit, the value of $\int_{-Z}^Z d^3Q \text{hd}! S(Q; !)$ for the 3.422 \AA bond is positive. This can only occur if this bond is geometrically frustrated. Frustration generally requires that antiferromagnetic bonds are arranged in triangles. As we will discuss below, the single crystal experiments suggest that multiple bonds in the 7- \AA range that are not resolved here are involved in the magnetic bond network in this system, and can provide the frustrating interactions for the 3.422 \AA bond.

B. Single Crystal Measurements

We now turn to the data obtained from inelastic scattering measurements on single crystals at $T = 1.6 \text{ K}$. Scans at constant wavevector were carried out at the locations in the $(h0l)$ plane of CuHPCl indicated in Fig. 4, as well as along the line $(1k0)$ perpendicular to this plane. Figures 5-9 show the data so obtained.

Inspection of this data set yields two important observations. First, there are at least two modes in the magnetic excitation spectrum of CuHPCl . This can be most easily seen at $Q = (1; 0.5; 0)$ in Fig. 5(c), where two resolution-limited peaks are clearly visible at $h! = 0.88$ and 1.2 meV. The two modes are also visible at other wavevectors such as $Q = (1.167; 0; 0)$ in Fig. 6(b). In addition in a number of scans, single peaks are observed that are significantly broader than the instrumental resolution. As will be discussed below, all of these scans are well-described by the superposition of two resolution-limited Gaussian peaks.

Strong evidence for the presence of more than one mode can also be obtained by noting that the magnetic excitation spectrum must have the symmetry $h!(Q) = h!(Q + \tau)$ where τ is a reciprocal lattice vector. As shown in Fig. 6(a), at $Q = (1; 0; 0)$ the spectrum is dominated by a strong peak at $h! = 0.87 \text{ meV}$. A peak at this energy is not observed at $Q = (1; 0; 1)$, but as shown in Fig. 7(c), a peak is seen instead at $h! = 1.2 \text{ meV}$. By the symmetry described above, there must be

modes at both of these energies at $Q = (1;0;0)$ and $Q = (1;0;1)$. Indeed, there is some evidence for the higher energy mode at $Q = (1;0;0)$, as indicated by the very weak peak at $h\omega = 1.2$ meV. The structure factors of the two modes evidently have different Q -dependence, and that of the lower mode yields zero scattering intensity at $Q = (1;0;1)$.

The second conclusion that can be drawn from inspection of the data relates to the dimensionality of the magnetic system in CuHPCl. A crucial signature of a low-dimensional spin system is the absence of dispersion in the magnetic excitations along directions in which there is no magnetic coupling. As may be seen from Fig. 5, there is no measurable dispersion of the low-energy mode at $h\omega = 0.87$ along $Q = (1;k;0)$. This indicates that magnetic excitations cannot propagate along the crystalline b direction. Possible reasons for this include the lack of a percolating network extending along b or geometrical frustration.⁴⁰

Turning to the $(h0l)$ plane, we first note that for a system of isolated spin-ladders running along $[101]$, there should be no dispersion of the magnetic excitations in the $(h;0;h)$ direction. This is not the case. As shown by the data in Fig. 8, the low-energy mode appearing at $h\omega = 0.87$ meV at $Q = (1;0;0)$ increases in energy along $(h;0;1-h)$, indicating the presence of magnetic coupling perpendicular to the ladders. Figures 6 and 9 show that there is also dispersion of this mode along $(h;0;0)$ and $(1;0;1)$. This still leaves the possibility of a one-dimensional system running along $[101]$, with no dispersion along $(h;0;h)$. However, if this were true, then the mode energies would have to be equal at $Q = (0.5;0;0.5)$ and at $Q = (1;0;1)$, and hence also at $Q = (1;0;0)$. As already noted, Figs. 6 and 8 show that the mode energies are different at $Q = (1;0;0)$ and $Q = (0.5;0;0.5)$, which rules out this possibility as well. Thus there is dispersion in all directions in the $(h0l)$ plane, and the spins in CuHPCl form a connected two-dimensional network in the ac plane.

To determine the energies and integrated intensities of the observed modes, we fit the magnetic scattering for each constant- Q scan to the sum of two Gaussian peaks. The width of the peaks was fixed at the instrumental energy resolution $\hbar\omega$. Effects of wavevector resolution are insignificant because of the low velocity of magnetic excitations in CuHPCl. The non-magnetic background was modeled by a constant term plus a third Gaussian where needed to account for the tail of the incoherent elastic scattering. The resulting fits are shown as solid lines in Figs. 5-9.

The energies of the modes derived in this way are shown in Figs. 10 and 11. The dispersion of the modes in all directions in the $(h0l)$ plane is clearly seen. In the absence of a detailed microscopic model of the true spin Hamiltonian for CuHPCl, we have parameterized the dispersion of each of the two modes in the $(h0l)$ plane with a phenomenological dispersion relation that satisfies Bloch's theorem:

$$h\omega(Q) = A_0 + A_1 \cos 2\pi h + A_2 \cos 2\pi l + A_3 \cos 2\pi (h+l) + A_4 \cos 2\pi (h-l); \quad (7)$$

The two maxima resolved in the magnetic density of states $\Gamma(\omega)$ (Fig. 2) provide some justification for the simplifying assumption that the modes do not cross. The solid lines in Figs. 10 and 11 show the fitted dispersion relations and the parameters for the fits are given in Table III.

The single-crystal data allow us to measure the angular dependence of the first moment of $S(Q; \omega)$, and hence to obtain further information about the geometry of the magnetic bonds in CuHPCl. Here we access the first moment $hh\omega_{\frac{1}{2}}$ of the full wavevector-dependent, normalized magnetic scattering intensity $\tilde{I}_m(Q; \omega)$, which is given by

$$hh\omega_{\frac{1}{2}} = \int_0^{\omega_{\frac{1}{2}}} \omega \tilde{I}_m(Q; \omega) d\omega = \frac{2}{3} \frac{g}{2} \int_0^{\omega_{\frac{1}{2}}} f(Q) \sum_d^X J_d \hbar S_0 \sin(1 - \cos Q \cdot d); \quad (8)$$

Here we have neglected any spin space anisotropy, a reasonable assumption for a spin-1/2 quantum spin liquid. In the present case, the first moment may be determined from the data as

$$hh\omega_{\frac{1}{2}} / \sum_i I_i \hbar \omega_{i1}; \quad (9)$$

where I_i and $\hbar \omega_{i1}$ are the set of integrated intensities and corresponding mode energies at each Q , and there is an undetermined overall scale factor since the data are not normalized.

The wavevector dependence of $hh\omega_{\frac{1}{2}}$ is illustrated in Fig. 4, in which the diameter of the data points is proportional to $hh\omega_{\frac{1}{2}}$, and is also shown in Figs. 12 and 13. This quantity is seen to be largest for the points along the line $(h;0;1-h)$. This is consistent with the powder data, as along this line the magnitude of Q is close to the value 0.55 \AA^{-1} where the peak in the powder first moment occurs (see Fig. 3). The strongest modulation in $hh\omega_{\frac{1}{2}}$ occurs along the (101) direction, with weaker modulation also visible in other directions. From the form of Eq. 8, this implies that the bond vector that contributes most strongly to the first moment points parallel to $[101]$. The only bonds that do this are those that form the legs of the ladders, Bonds 4 and 6 in Table I. To test this, we modeled the measured first moment with Eq. 8, using up to three Cu-Cu bonds with length $d < 10 \text{ \AA}$. Indeed, either Bond 4 or Bond 6 gives the dominant contribution to the models that yield the best results. As may be seen in Table I, these bonds are nearly identical, and the present data set cannot distinguish between them. There are three other pairs of nearly identical bonds among the those listed in Table I: Bonds 5 and 7, Bonds 8 and 10, and Bonds 9 and 11. Essentially identical fits to the data are provided by those three-bond models that include one

of Bonds 4 and 6, one of Bonds 5 and 7, and one of Bonds 8 and 10. These are measurably better, however, than all other bond combinations. The t using Bonds 5, 6, and 8 is shown in Figs. 12 and 13, and the parameters are given in Table IV. As will be discussed below, Bonds 5, 7, 8 and 10 couple the ladders in the a-c plane. We note that frustration of Bond 8 or 10 is always indicated in the set of equivalent three-bond models.

IV. DISCUSSION

The information obtained from the measurements presented here about the geometry of the spin-coupling in CuHPCl may be summarized as follows. The powder data show that the dominant bond length is in the range $d = 7.8 \text{ \AA}$, and that the rung bond of the ladders with $d_1 = 3.422 \text{ \AA}$ is frustrated. The single-crystal data show that the system is quasi-two-dimensional, with two magnetic modes that show dispersion in all directions in the a-c plane, and weaker dispersion perpendicular to this plane. These data show that the dominant bond is one of the leg bonds of the ladders that are nearly parallel to [01], and also show contributions from bonds that can provide coupling between the ladders in the a-c plane. Thus, a system of magnetically isolated, one-dimensional spin ladders is not the appropriate microscopic spin Hamiltonian for CuHPCl.

Figure 14 (a) shows a projection of the crystal structure of CuHPCl, looking down the [01] (former ladder) axis. Although CuHPCl is not magnetically a spin ladder, we shall continue to use this term in the following to refer to the structural unit of the material. The "inter-ladder" bonds 5, 7, 8 and 10 lie in buckled sheets in the a-c plane indicated by solid lines in Fig. 14 (a), and couple the top leg of each ladder to the bottom legs of the neighboring ladders. A view of one of these sheets, looking down the [010] axis is shown in Fig. 14 (b). Bonds 4-8 and 10 form a distorted triangular lattice, which can explain the source of the frustration indicated for Bonds 8 and/or 10 in the analysis of the single-crystal data. On the basis of the first moment data, either of the two ladder-leg bonds, Bonds 4 and 6, could form the strong bond (dimer). These bonds involve very similar Cu-N-H-C-H-Cu linkages,¹⁴ but they cannot both be strong and of equal strength, as that would create a system of extended, uniform $S=1/2$ chains which would not have a spin-gap. Similarly, Bonds 8 and 10 would form uniform chains along [100] if both were strong. Bonds 5 and 7 must also be inter-dimer bonds, as these individually form extended chains along [001].

The frustration of Bond 1 indicated by the powder data requires that bonds other than Bonds 4-8 and 10 be present, as these alone do not provide a local triangular network involving Bond 1. One possibility is that there are additional Cu-Cu couplings within individual ladders, as could be provided by Bonds 2 and 3. How-

ever, there is no evidence for these bonds in our data. Another possibility may be seen from Fig. 15. This view along (010) shows a network in the a-b plane that involves Bonds 8-11 and Bond 1, and could also provide the frustration we observe. Such a network is consistent with the powder data, as it only involves bonds in the 7- \AA range in addition to Bond 1. The single crystal data, however, does not allow us to assess the validity of this model, as the small amount of data out of the (h0l) plane provides only limited information about Bonds such as 1, 9, and 11 that have major components along [010]. Indeed, other possible frustrated networks exist in this structure. For example, a very similar network to that in Fig. 15 exists in the b-c plane, although it involves bonds longer than 8 \AA . In the end, although the present results show that the spin coupling in CuHPCl is at least two-dimensional and provide strong constraints on the identity of the dimer bond, the data are not of sufficient quality to determine fully the microscopic spin Hamiltonian of this material. In particular, measurements would have to be carried out on single crystals over a larger region of reciprocal space to distinguish among the large number of possible secondary spin couplings.

V. SUMMARY

In summary, we have presented inelastic neutron scattering data from deuterated powder and hydrogenated single crystals of the gapped quantum antiferromagnet CuHPCl. Our results show that while the system is well-described by a collection of weakly interacting dimers, the magnetic coupling between the dimers is not that of a one-dimensional spin-ladder, but is at least two-dimensional. Our results further suggest that geometrical frustration may play an important role. It should be interesting to re-assess the large body of existing experimental data for this material in light of this new information.

VI. ACKNOWLEDGMENTS

We thank R. Paul for help with neutron activation analysis. This work was supported by NSF Grant DMR-9801742. DHR acknowledges the support of the David and Lucile Packard Foundation. TL acknowledges the support of the Sloan and Dreyfus Foundations. X-ray characterization was carried out using facilities maintained by the JHU MRSEC under NSF Grant number DMR-0080031. This work utilized neutron research facilities supported by NIST and the NSF under Agreement No. DMR-9986442.

- ¹ G. Xu, C. Broholm, D. H. Reich, and M. A. Adams, Phys. Rev. Lett. 84, 4465 (2000).
- ² D. C. Johnston, J. W. Johnson, D. P. Goshorn, and A. J. Jacobson, Phys. Rev. B 35, 219 (1987).
- ³ R. S. Eccleston, T. Barnes, J. Brody, and J. W. Johnson, Phys. Rev. Lett. 73, 2626 (1994).
- ⁴ A. W. Garrett, S. E. Nagler, T. Barnes, and B. C. Sales, Phys. Rev. B 55, 3631 (1997).
- ⁵ A. W. Garrett, S. E. Nagler, D. A. Tennant, B. C. Sales, and T. Barnes, Phys. Rev. Lett. 79, 745 (1997).
- ⁶ S. A. Carter, B. Batlogg, R. J. Cava, J. J. Krawski, W. F. Peck, Jr., and T. M. Rice, Phys. Rev. Lett. 77, 1378 (1996).
- ⁷ R. S. Eccleston, M. Uehara, J. A. Kinoshita, H. Eisaki, N. Motoyama, and S. Uchida, Phys. Rev. Lett. 81, 1702 (1998).
- ⁸ M. Matsuda, T. Yoshimura, K. Kakurai, and G. Shirane, Phys. Rev. B 59, 1060 (1999).
- ⁹ B. Leuenberger, A. Stebler, H. U. Gudel, A. Furrer, R. Feile, and J. Krawski, Phys. Rev. B 30, 6300 (1984).
- ¹⁰ Y. Sasago, K. Uchinokura, A. Zheludev, and G. Shirane, Phys. Rev. B 55, 8357 (1997).
- ¹¹ N. Cavadin, W. Henggeler, A. Furrer, H. U. Gudel, K. Kramer, and H. Muta, Euro. Phys. J. B 7, 519 (1999).
- ¹² M. B. Stone, I. Zaliznyak, D. H. Reich, and C. Broholm, unpublished.
- ¹³ H. Kageyama, K. Yoshimura, R. Stem, N. V. M ushnikov, K. Onizuka, M. Kato, K. Kosuge, C. P. Slichter, T. Goto, and Y. Ueda, Phys. Rev. Lett. 82, 3168 (1999).
- ¹⁴ B. Chiari, O. Piovesana, T. Tarantelli, and P. F. Zanazzi, Inorg. Chem. 29, 1172 (1990).
- ¹⁵ P. R. Hammar and D. H. Reich, J. App. Phys. 79, 5392 (1996).
- ¹⁶ G. Chaboussant, P. A. Crowell, L. P. Levy, O. Piovesana, A. Madouri, D. Mailly, Phys. Rev. B 55, 3046 (1997).
- ¹⁷ G. Chaboussant, M. Julien, Y. Fagot-Reverat, L. P. Levy, C. Berthier, M. Horvatic, and O. Piovesana, Phys. Rev. Lett. 79, 925 (1997).
- ¹⁸ G. Chaboussant, M. Julien, Y. Fagot-Reverat, M. E. Hanson, C. Berthier, M. Horvatic, L. P. Levy, and O. Piovesana, Phys. Rev. Lett. 80, 2713 (1998).
- ¹⁹ P. R. Hammar, D. H. Reich, C. Broholm, and F. Trouw, Phys. Rev. B 57, 7846 (1998).
- ²⁰ G. Chaboussant, M. Julien, Y. Fagot-Reverat, M. Hanson, L. P. Levy, C. Berthier, M. Horvatic, and O. Piovesana, Euro. Phys. J. B 6, 167 (1998).
- ²¹ M. Chiba, T. Fukui, Y. Ajiro, M. Hagiwara, T. Goto, and T. Kubo, Physica B 246-247, 576 (1998).
- ²² M. Hagiwara, Y. Nanumi, K. Kindo, T. Nishida, M. Kaburagi, and T. Tonegawa, Physica B 246-247, 234 (1998).
- ²³ H. Deguchi, S. Sumoto, S. Takagi, M. Mito, T. Kawae, K. Takeda, H. Nojiri, T. Sakon, and M. Motokawa, J. Phys. Soc. Jpn. 67, 3707 (1998).
- ²⁴ R. Calmcsuk, J. Riera, D. Poilblanc, J.-P. Boucher, G. Chaboussant, L. P. Levy, and O. Piovesana, Euro. Phys. J. B 7, 171 (1999).
- ²⁵ H. Ohta, T. Tanaka, S. Okubo, S. Kimura, H. Kikuchi, and H. Nagasawa, J. Phys. Soc. Jpn. 68, 732 (1999).
- ²⁶ G. Chaboussant, M. Julien, Y. Fagot-Reverat, M. Moya, M. Horvatic, L. P. Levy, C. Berthier, and O. Piovesana, Physica B 280, 315 (2000).
- ²⁷ H. Moya, M. Horvatic, C. Berthier, M. Julien, P. Segransan, L. Levy, and O. Piovesana, Phys. Rev. Lett. 85, 4795 (2000).
- ²⁸ N. Elstner, and R. R. P. Singh, Phys. Rev. B 58, 11484 (1998).
- ²⁹ T. Giamarchi and A. M. Tsvelik, Phys. Rev. B 59, 11398 (1999).
- ³⁰ X. Wang and L. Yu, Phys. Rev. Lett. 84, 5399 (2000).
- ³¹ B. Normand, J. Kyriakidis, and D. Loss, Ann. Phys. Berlin 9, 133 (2000).
- ³² C. A. Hayward, D. Poilblanc, and L. P. Levy, Phys. Rev. B 54, R12649 (1996).
- ³³ M. Usami and S. Suga, Phys. Rev. B 58, 14401 (1998).
- ³⁴ Q. Gu and J. Shen, Phys. Lett. A 251, 150 (1999).
- ³⁵ Q. Gu, D. Yu, J. Shen, Phys. Rev. B 60, 3009 (1999).
- ³⁶ Z. Weihong, R. R. P. Singh, and J. Oitmaa, Phys. Rev. B 55, 8052 (1997).
- ³⁷ Chem. Abstr. 70, 57917d (1969).
- ³⁸ N. D. Chesser and J. D. Axe, Acta Cryst. Sect. A 29, 160 (1973).
- ³⁹ P. C. Hohenberg, W. F. Brinkman, Phys. Rev. B 10, 128 (1974).
- ⁴⁰ K. Kakurai et al., J. Phys. Chem. Solids 62, 141 (2001).

Bond Number	d (Å)	x/a	y/b	z/c
1	3.422	0.179	0.231	0.089
2	5.774	0.331	0.234	0.399
3	5.822	0.312	0.227	0.423
4	6.996	0.509	0.003	0.488
5	6.998	0	0.266	0.5
6	7.002	0.491	0.003	0.512
7	7.033	0	0.273	0.5
8	7.206	0.491	0.269	0.012
9	7.393	0.312	0.5	0.077
10	7.552	0.509	0.269	0.012
11	7.672	0.331	0.5	0.101

TABLE I. Cu-Cu Bond lengths and fractional coordinates for CuHfPc₁ calculated from previously determined atomic coordinates.¹⁴ Bonds 1 and 4-11 are illustrated in Figs. 14-15.

Number of bonds	d	$J d \hbar S_0$	$\$i$ (m eV)	d	$J d \hbar S_0$	$\$i$ (m eV)
1	7.5 (2)	-0.82 (1)				
2	7.5 (1)	-1.15 (3)		3.422	0.36 (3)	

TABLE II. Bond lengths and corresponding $J d \hbar S_0$ $\$i$ terms determined by fitting first moment of powder data to a single bond length, and also to two bond lengths such that $d = d_1$.

Dispersion parameter	lower mode (m eV)	upper mode (m eV)
A_0	1.00 (2)	1.21 (2)
A_1	-0.04 (2)	-0.03 (2)
A_2	-0.02 (2)	0.00 (2)
A_3	-0.07 (2)	0.01 (2)
A_4	-0.02 (2)	-0.03 (2)

TABLE III. Parameters determined from phenomenological fit to measured dispersion in CuHpCl using Eq. 7.

Bond	$J d \hbar S_0$	$\$i$	Bond	$J d \hbar S_0$	$\$i$	Bond	$J d \hbar S_0$	$\$i$
5	-2.9 (5)		6	-4.5 (5)		8	1.5 (6)	

TABLE IV. Fit parameters for a three bond fit to the single crystal first moment data. $J d \hbar S_0$ $\$i$ values are in arbitrary units. Bond numbers correspond to those listed in Table I. The first moment calculated using these parameters is shown as the solid line in Figs. 12 and 13.

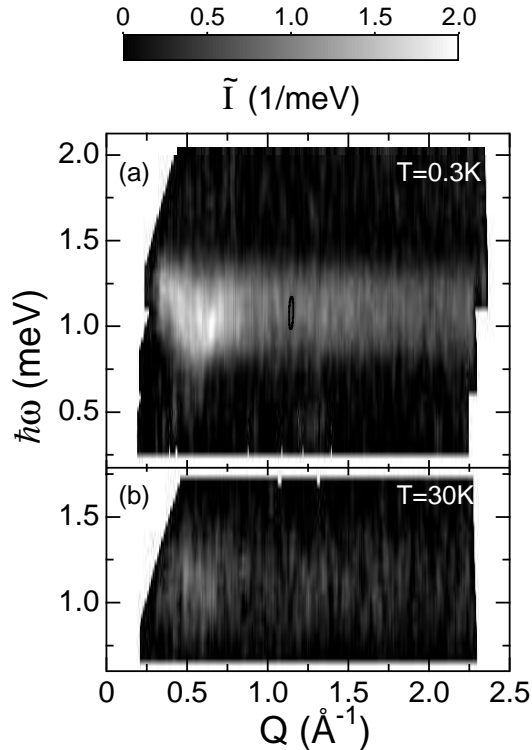


FIG. 1. Powder inelastic neutron scattering intensity $I(Q; \hbar\omega)$ for CuHpCl at (a) $T = 0.3$ K, and (b) $T = 30$ K. The FWHM resolution ellipse is depicted in panel (a).

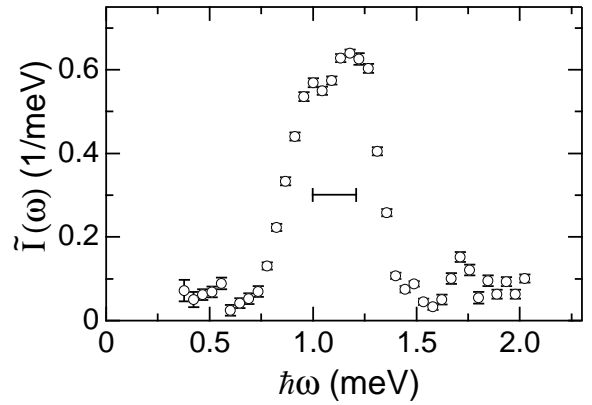


FIG. 2. Wavevector-averaged scattering intensity vs. energy transfer for CuHpCl. The region of integration is limited to $0.3 \text{ \AA}^{-1} < Q < 2.3 \text{ \AA}^{-1}$. The horizontal bar indicates the FWHM energy resolution.

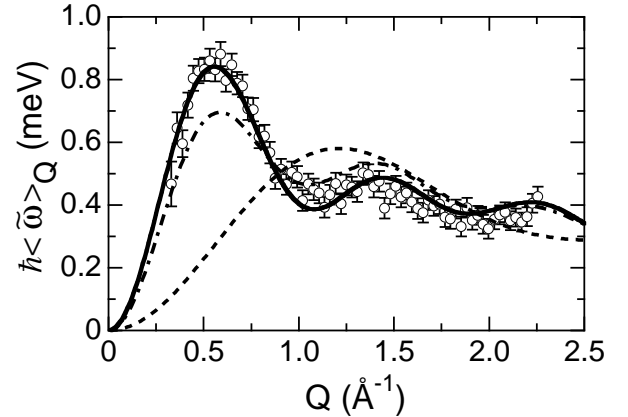


FIG. 3. First moment of the energy-integrated intensity vs. wavevector transfer for CuHpCl. The region of integration is limited to the band of magnetic excitations from 0.7 to 1.5 meV. The dashed-dotted line is a fit with a single dimer bond length of 7.5 (2) Å. The dashed line is a fit using the dimer bond length to 3.422 Å, as expected in the spin-ladder model. The solid line is the best fit using two Cu-Cu bond lengths as described in the text. Fit results are described in the text and enumerated in Table II.

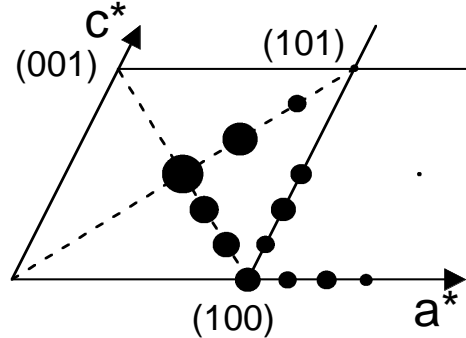


FIG. 4. Locations in the $(h0l)$ plane at which single-crystal inelastic neutron scattering data was obtained for CuHpCl. The diameter of the points is proportional to the measured first moment of the data, and shows that the strongest magnetic bond is parallel to $[101]$.

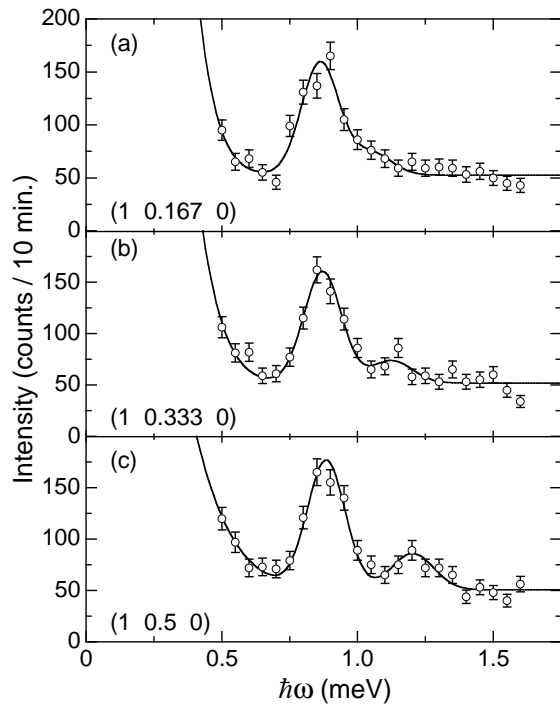


FIG. 5. Inelastic neutron scattering data for CuHPCl indicating a lack of dispersion along the $(1k0)$ direction. The scan at $(1;0.5;0)$ shows the presence of two modes in the excitation spectrum. Solid lines are fits as described in the text.

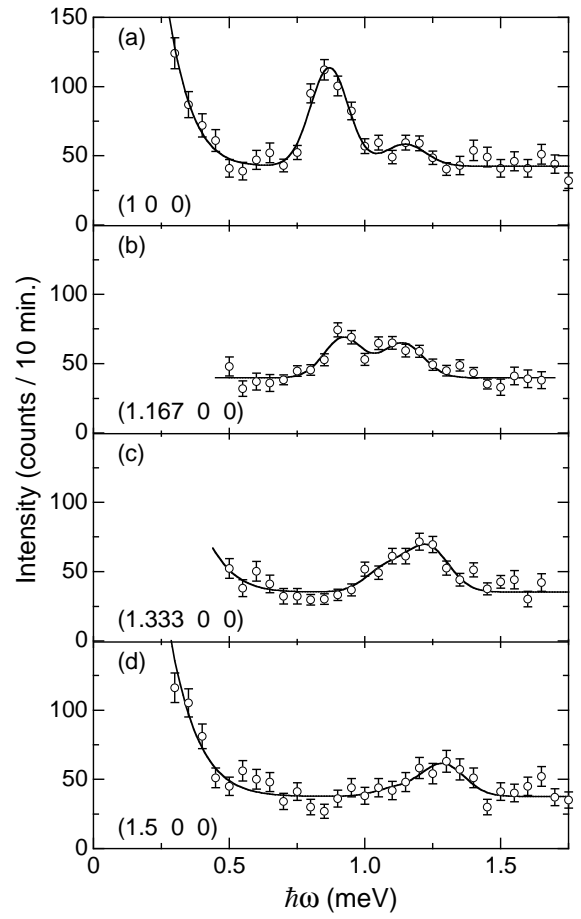


FIG. 6. Inelastic neutron scattering data for CuHPCl indicating dispersion along the $(h00)$ direction. Solid lines are fits as described in the text.

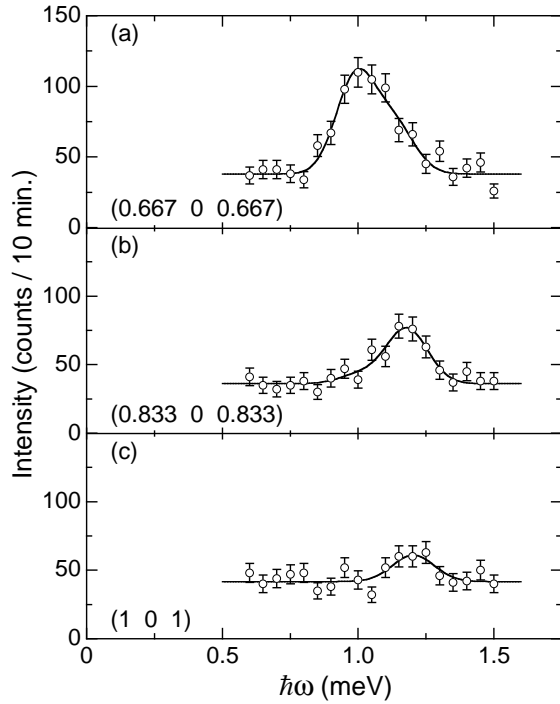


FIG. 7. Inelastic neutron scattering data for CuHPCl indicating dispersion along the $(h0h)$ direction. Solid lines are fits as described in the text.

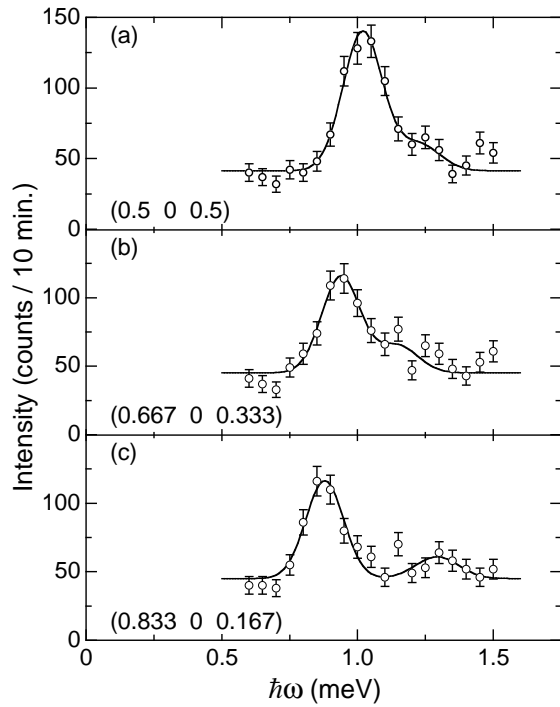


FIG. 8. Inelastic neutron scattering data for CuHPCl indicating dispersion along the $(h;0;1-h)$ direction, perpendicular to the putative spin ladder direction. Solid lines are fits as described in the text.

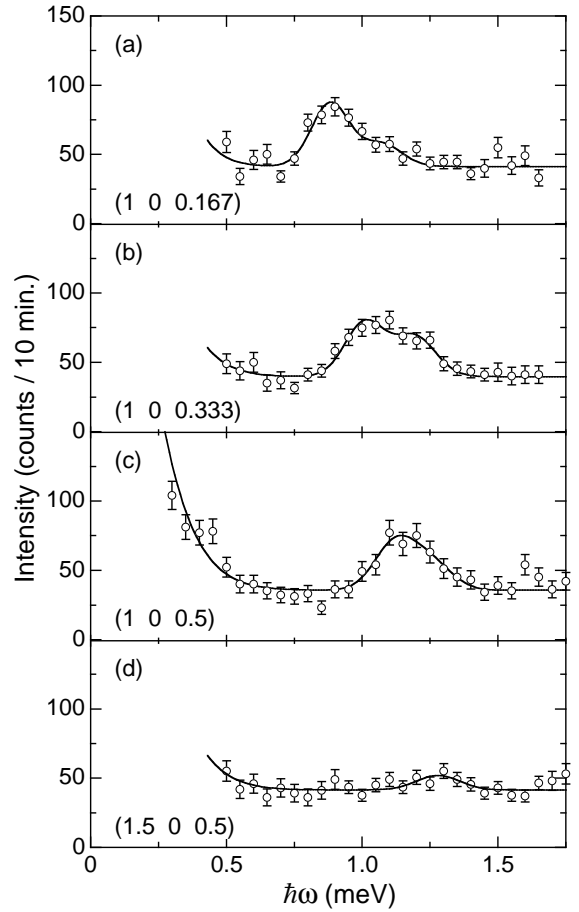


FIG. 9. Inelastic neutron scattering data for CuHPCl. (a)-(c) show dispersion along the $(10l)$ direction. Solid lines are fits as described in the text.

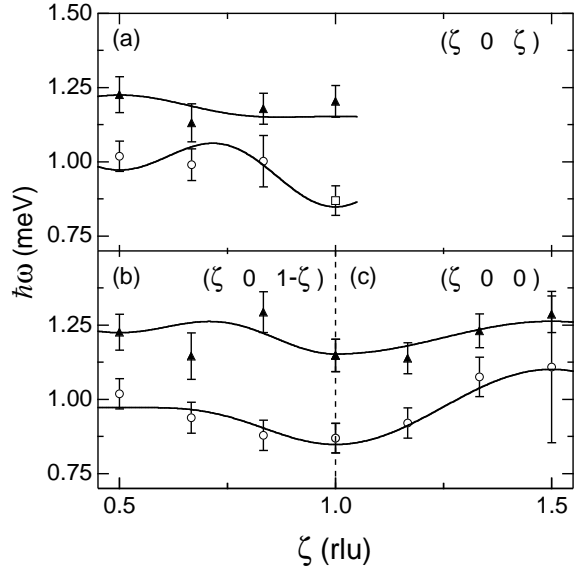


FIG. 10. Dispersion of magnetic excitations in CuH-pCl for the data shown in Figs. 6, 7, and 8. Open circles represent the lower energy mode, solid triangles represent the higher energy mode, and the open square point at (101) represents the energy of the dominant mode at (100) translated by $\gamma = (001)$. Lines are phenomenological fits as described in the text.

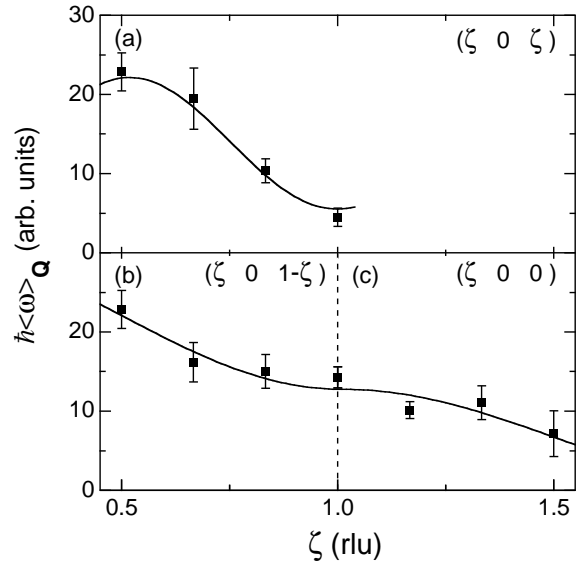


FIG. 12. First moment of the magnetic excitations in CuH-pCl derived from single-crystal data. Curves are fits as described in text.

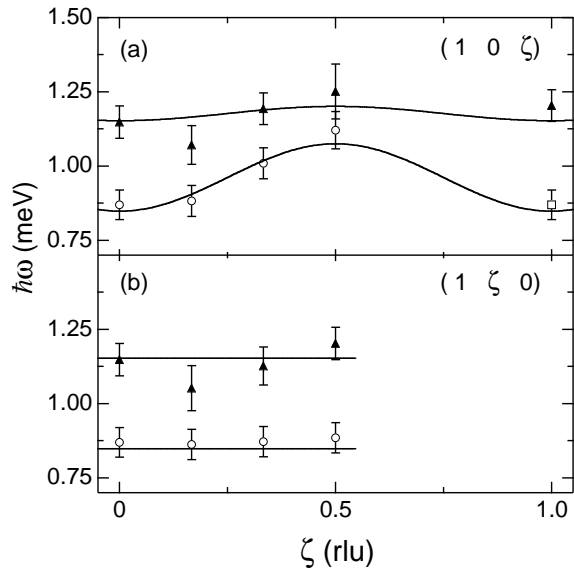


FIG. 11. Dispersion of magnetic excitations in CuH-pCl for the data shown in Figs. 5 and 9. Open circles represent the lower energy mode, solid triangles represent the higher energy mode, and the open square point at (101) represents the energy of the dominant mode at (100) translated by $\gamma = (001)$. Solid lines are phenomenological fits as described in the text.

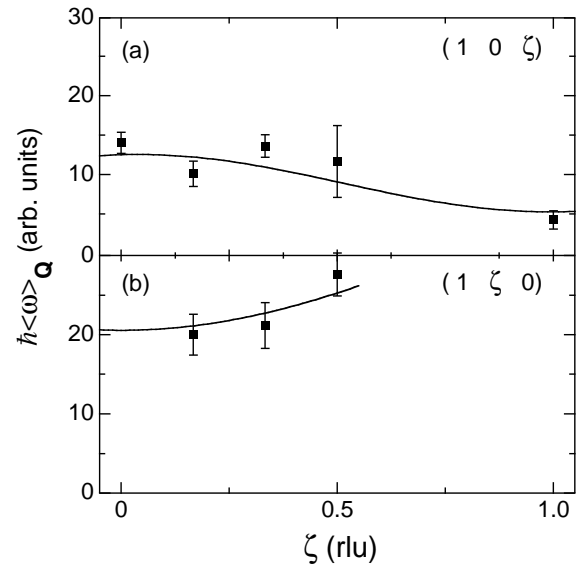


FIG. 13. First moment of the magnetic excitations in CuH-pCl derived from single-crystal data. Curves are fits as described in text. The (1 0) curve has been scaled due to the change in sample illumination for the points along this curve.

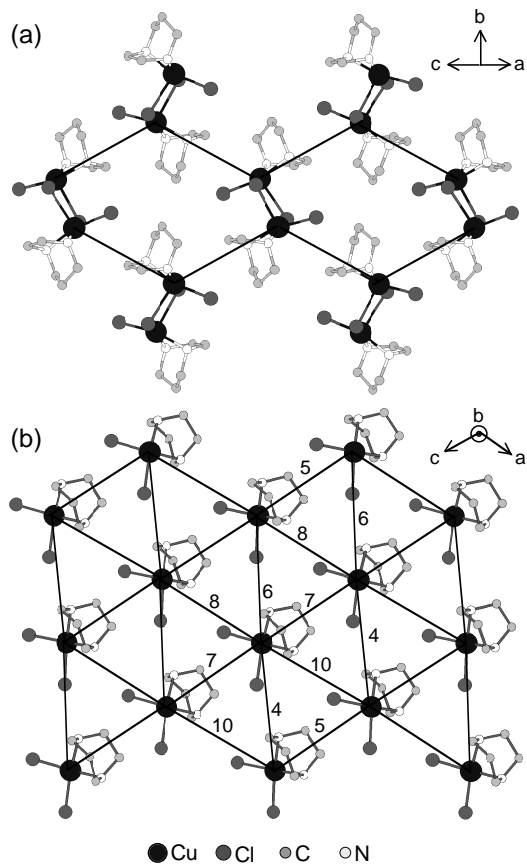


FIG .14. (a) Crystal structure of CuHpCl as viewed down the [101] axis. The solid lines show the locations of Cu-Cu bonds 5,7,8, and 10 (see Table I). In this view, these bonds appear behind one another in the crystal lattice. (b) View looking down [010]. Cu-Cu bonds 5-8 and 10 are as listed in Table I. The network in (b) corresponds to the upper half of the crystal structure shown in (a).

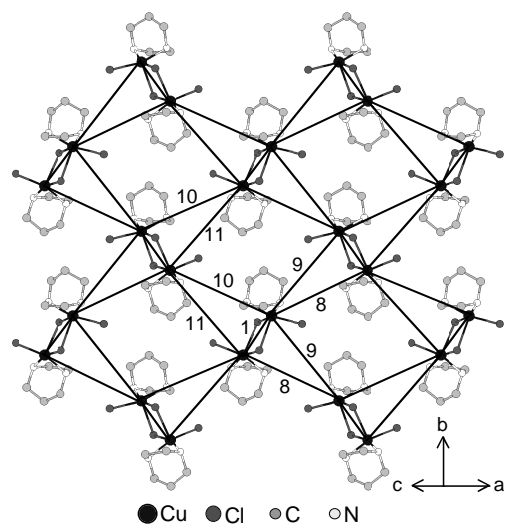


FIG .15. Crystal structure of CuHpCl as viewed down (010) axis, showing possible frustrated bond network. Bonds 8-11 are as listed in Table I.